Defence Science Journal, Vol. 71, No. 1, January 2021, pp. 124-133, DOI : 10.14429/dsj.71.15557

Study on System Design and Integration of Variable Buoyancy Systems for Underwater Operation

B.K. Tiwari and R. Sharma*

Department of Ocean Engineering, Indian Institute of Technology Madras, Chennai - 600 036, India
**E-mail: rajivatri@iitm.ac.in*

ABSTRACT

This paper presents the design and analysis of the 'Variable Buoyancy System (VBS)' for depth control which is an essential operation for all underwater vehicles. We use the 'Water Hydraulic Variable Buoyancy System (WHVBS)' method to control the buoyancy and discuss details of the system design architecture of various components of VBS. The buoyancy capacity of the developed VBS is five kilograms and the performance of the VBS in standalone mode is analysed using numerical simulation. Presented VBS is operable to control the buoyancy up to sixty meters of depth and it can be directly installed to medium size UVs. Simulation results show that the developed VBS can reduce the energy consumption significantly and higher in each cycle (i.e. descending and ascending) of the same VBS in standalone mode being operated with either propeller or thruster for sixty meters depth of operation. Our results conclude and demonstrate that the designed VBS is effective in changing the buoyancy and controlling the heave velocity efficiently and this serves the purpose of higher endurance and better performances desired in rescue/attack operations related to the UVs both in civilian and defense domains.

Keywords: Autonomous underwater vehicle /glider; Variable buoyancy system; Positive displacement pump; Underwater vehicle; Water hydraulic variable buoyancy system

NOMENCLATURE

a	Acceleration of the VBS in m/s^2
A_p	Projected area in m^2
ΔB	Change in buoyancy in kg
C_D	Coefficient of drag
E	Energy in joules
E_m	Elastic modulus
E_0	No load energy required in joules
g	Gravitational acceleration in m/s^2
H_{op}	Operating depth in m
K_{edc}	Effective drag coefficient in watt-s^3 /m^3
m	Mass of the VBS in kg
m_a	Added mass in kg
P_a	Atmospheric pressure in N/m^2
P_{cr}	Critical pressure acting on the VBS in N/m^2
P_h	Hotel load in watt
R	Range in m
R_m	Mean radius of the ballast tank
t	Thickness of the ballast tank in m
U	Velocity in m/s
V_{di}	Displaced volume by the VBS in m^3
V_{inner}	Inner volume of the ballast tank in m^3
V_s	Sensor output voltage in volt
V_{ff}	Volume of the fluid filled inside the ballast tank in m^3
w	Heave velocity in m/s
ρ_f	Fluid density (in this study it sea water) in kg/m^3
η_v	Volumetric efficiency of the ballast tank
ν	Poisson's ratio of the materials

Received : 05 March 2020, Revised : 21 July 2020
Accepted : 18 September 2020, Online published : 01 February 2021

1. INTRODUCTION

A large part of the oceans/seas existing on earth's surface remains unexplored and need to be explored and investigated for marine natural resources such as oil and gas, ocean creature habitats, weather/climate patterns, underwater mining, cabling, and defence purposes, etc., for more details see Tiwari & Sharma[1]. Although the ocean can be explored by surface vehicles and underwater vehicles, to avoid risks to human lives and to bring in more autonomy/artificial intelligence into the design, operation, and surveys, the recent focus has shifted towards the Autonomous Underwater Vehicles/Gliders (i.e. AUVs/Gs). These AUVs/Gs can be either with a propeller or without propeller and are unmanned, an untethered underwater vehicle capable of carrying out simple activities with little or no human supervision. The ability to perform without human or with little interventions has allowed the AUVs/Gs to offer a wide range of applications in scientific, military, commercial, and policy sectors. Additionally, their ability to operate autonomously of a parent vessel makes them preferable for the exploration of extreme marine environments. We believe that the possible incorporation of goals of artificial intelligence including reasoning, knowledge representation, planning, learning, natural language processing, perception, and the ability to move and manipulate objects is expected to revolutionise our abilities in marine robotic applications. In the future, these are expected to include image/measure/survey/map the seafloor and marine environment providing higher resolution data that cannot be achieved from surface vessels, particularly in deep water.

These UVs are applicable for the underwater survey without or with little human intervention during the operation of the vehicles. However, their high energy consumption required for the hovering, descending, and ascending, adversely affects their performance such as range and endurance[2]. If we increase the energy storage capacity installed in the AUV, as shown in Fig. 1, then the ratio of the mass of the power source (i.e. battery) to the total mass of the AUV will extend from 10 to 40 percent, depending upon the requirements for various existing vehicles. This addition of mass affects the overall payload, is highly undesired, and limits the payload capacities such as various sensors (e.g. optical sensors, electromagnetic sensors, CTD sensors, and electromagnetic sensors, etc.).

We note that the use of the 'Variable Buoyancy System (VBS)' will minimise the energy consumption during the AUVs operations and increase the performance such as range and endurance as well as the payload, for more details see Tiwari and Sharma[1]. Because of these reasons, it is important that the design and development of VBS for UVs are investigated and the results made available in the public domain.

2. FUNCTIONAL REQUIREMENT ANALYSIS OF THE VBS

Following the Bradley[4], *et al.,* the range (R) of underwater vehicles is defined as follows:

$$R = \frac{E \times U}{K_{edc} \times U^3 + P_h} \tag{1}$$

where K_{edc} is the effective drag coefficient in watt-s^3/m^3 acting on the vehicle, E is the energy stored in the vehicle in Joules used only for the propulsion of the vehicle, U is the velocity and P_h is the hotel load. In Eqn (1) the K_{edc} can be computed as follows:

$$K_{edc} = \rho_f A_p C_D / 2 \tag{2}$$

where ρ_f is the density of the fluid (i.e. in our application liquid), A_p is the projected area of the vehicle and C_D is the drag coefficient. Numerical simulation has been performed with the assumption of a simplified form of the vehicle, and we neglect the wave force, hydrodynamic force, current effects, and Coriolis forces. Other simulation parameters are: C_D = 0.8, ρ_f as the fluid density (i.e. seawater) 1025 kg/m^3, and the projected area A_p = 1.28 m^2 based on the consideration of 3.0 m length of the the vehicle and maximum diameter as 0.426 m.

We note that the power required to overcome the drag of the vehicle is proportional to the cubic power of velocity. So if the velocity is increasing then the range will decrease at a faster rate at a given amount of energy stored for the vehicle and if the velocity is reducing to very low values (i.e. tends to become zero at no hotel load condition) then the range will tend to become indeterminate, e.g. infinite. In our work, under the condition of no hotel load, we consider the example of three different energy capacities, i.e. 15, 20, and 25 kJ for the propulsion of the AUV, and the lowest operating velocity considered is 0.25 m/s. As the velocity is on the lower side the power required to overcome drag is very less and because of this the range increases, i.e. 560 m, 740, and 930 m are achieved as shown in Fig. 2 (a). If further, we reduce the velocity to even lower than 0.25 m/s in the range of $0 < U \le 0.25 m/s$,

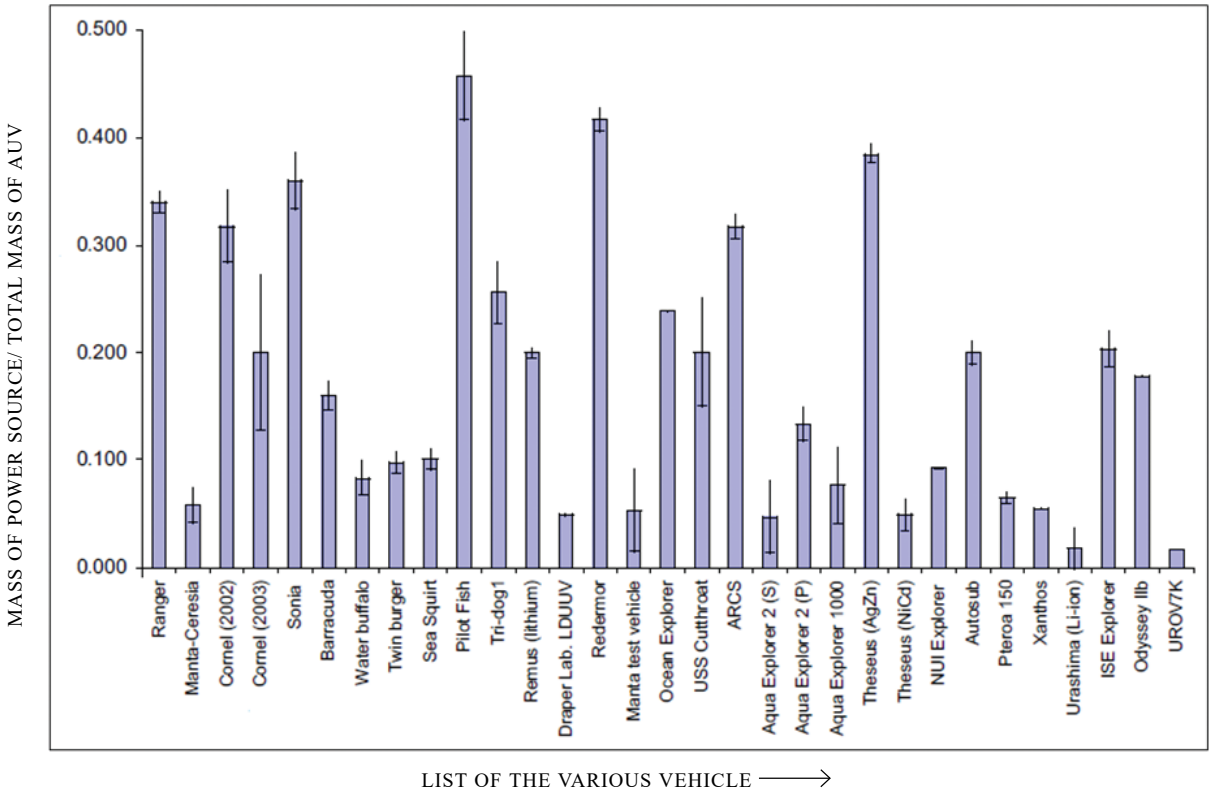

Figure 1. Ratio of the mass of the power source to the mass of the AUVs for different vehicles adapted from Griffiths[3], *et al.*

then the power required to overcome drag reduces rapidly. Because of this, the range will tend to be very high in the range of $0 < U \leq 0.25\,m/s$ in no hotel load condition.

Higher hotel load adversely affects the range of the vehicle and higher energy storage offers a higher range for the same hotel load as shown in Fig. 3. For velocity around $0 < U \leq 0.25\,m/s$, the range increases with an increase in the velocity, and beyond that, it decreases non-linearly because the power required to overcome the drag is a cubic function of the velocity. Furthermore, we can observe from Figs. 2 (a) and 2 (b) that range with hotel load at high speed is higher than without hotel load. This is due to the assumption of high energy storage of 70 kJ with hotel load than 15, 20, and 25 kJ of energy without hotel load. Herein, we have not considered the same amount of onboard energy on the vehicle and the idea is to achieve the maximum range of 800 m in both the conditions, i.e. without hotel load range of 800 m can be achieved with 25 kJ stored energy and with hotel load this stored energy requirement will be 70 kJ. We note that to achieve the operating range of more than 200 m, for no hotel load condition energy storage should be greater than 25 kJ at the velocity above the 0.4 m/s and with given hotel load condition at speed above the 0.8 m/s energy must be greater than 70 kJ to achieve the operating range of more than 200 m. This analysis highlights the critical need for high energy storage and it also pushes the mass of the power source upwards while affecting the payload adversely.

Given the above discussion, an alternate approach is needed, e.g. to use the VBS. We note from the pieces of literature: Seahorse[5] AUV (length of 8.5 m) integrated with very large buoyancy capacity of (B = ±90 kg); URASHIMA AUV (length of 10.6 m) developed by JAMSTEC designed for 50 liters of oil transferable through a rubber bladder to change buoyancy[6] and rated depth of 3500 m; and Theses[7] AUV (length of 10.7 m) which has a safe working depth of 1000 m and integrated with VBS of 95 kg buoyancy capacity.

Furthermore, buoyancy controlled based on the hydraulic method (i.e. oil as a working medium for buoyancy control) by the change in the displaced volume of the external bladder[8-10] has been discussed as a short design summary. Wang[11], *et al.* discussed both hydraulic and pneumatic buoyancy control methods. In the UVs of size, less than 2 m in length - AUGs - some of the gliders (i.e. Sea and Spray gliders[12-13]) control their buoyancy by changing the displaced volume of the external bladders. Also, some other approaches to control of buoyancy include changing the volume of metal bellows[14-15] either by operating an electric linear actuator or using paraffin wax with a Peltier device method to control the buoyancy. In Slocum glider, a single-stroke displacement piston pump was used with a rolling diaphragm seal to move water and control its buoyancy by changing the overall mass of the glider. We note here that all these methods for AUGs are limited to very low capacity of buoyancy change, i.e. less than 260 ml, and maximum possible displaced volume capacities are limited to 900 cc.

Sumantr[16], *et al.* presented a design summary of the variable ballast mechanism for 'Underwater Robotic Vehicle (URV)' and this design has a movable plate inside the ballast

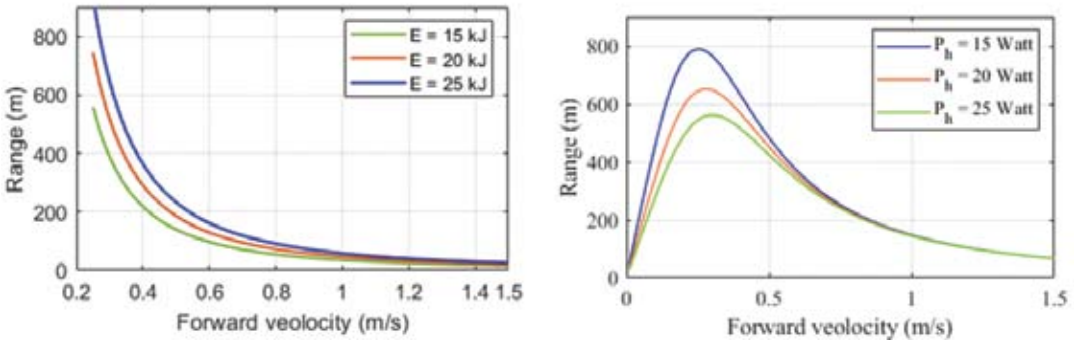

(a) (b)

Figure 2. Forward propulsive velocity of AUV versus the range for different onboard stored energies. (a) Without hotel load and (b) With hotel load.

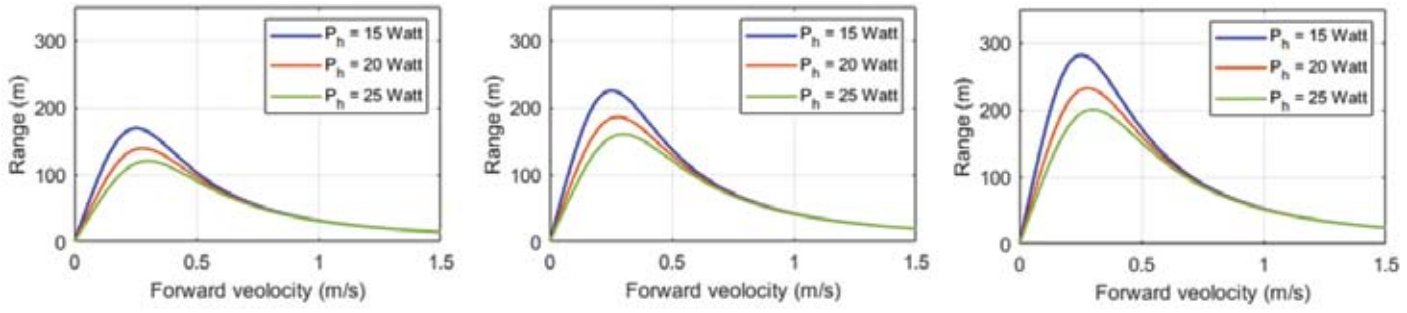

(a) (b) (c)

Figure 3. Propulsive velocity of AUV versus the range with hotel load. (a) For onboard storage energy E = 15 kJ, (b) For E = 20 kJ and (c) For E = 25 kJ.

tank. Movement of the plate results into the variable volume of the ballast tank filled with water to control the total mass of the vehicle hence the buoyancy. This system is similar to the piston operated VBS and is known to suffer from high mechanical complexity and low efficiency. Performance and stability study of the AUV by relatively changing the buoyancy and mass center for various buoyancy capacities UVs were analysed in Zhang[17], *et al.* and Ayyangar[18], *et al.*. Wang[19], *et al.* investigated the influence of the change in density of the seawater and advocated the use of the buoyancy compensator (i.e. VBS) to counter it.

Despite the existence of various buoyancy control methods from quite some time, there exist very limited information available in the public domain about their design process, details on scalability in design, and various components. In their absence, an application of VBS across different ranges of operating depths is not possible. Our work addresses these limitations and we present a design approach that is scalable and lists the detailed design components of VBS. Additionally, on a critical note, we observe that a complete design approach of VBS for small to medium to the large size of the AUV (i.e. herein focus is on $3.0 \leq L_{AUV} \leq 6.0$), and for comparatively large buoyancy capacity change is not available in the public domain. This study is aimed at filling this research gap.

3. DETAILED DESIGN METHODOLOGY AND ANALYSIS OF VBS

Typically, a VBS consists of distinct components, i.e. spherical ballast tanks, Positive Displacement Pump (PDP) to fill/remove the fluid, electric brushless motor required to run the pump, Li-ion based power source, control one-way valves, and water level sensors, etc. Fig. 4 shows the detailed system architecture of various components of the VBS. Overall these are classified into: System 1 - Structural systems composed of the ballast tank (water/oil storage tank), compressed air chamber or metal bellows, etc. for expanding/contraction to control the buoyancy; System 2- Electronic components include water level sensor, flow sensor, microcontroller (e.g. Aurduino Uno), power source and data logging systems, and System 3 - Mechanical systems which are composed of the pumps, check valve and flow direction control valves, etc.

To analyse the structural system of the VBS, we start with the type of the ballast tanks, e.g. selection of the ballast tanks (i.e. spherical/cylindrical) is a function of the method used to control the buoyancy. In the UVs, normally cylindrical tanks are used for piston-driven (i.e. syringe actuated) VBS and are

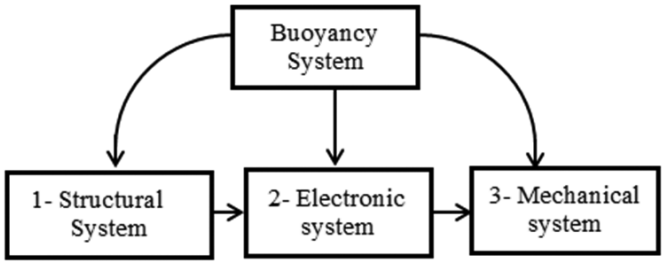

Figure 4. System architecture of various components of the VBS.

applicable for low buoyancy changes that too at low water depths because of the required high thrust at the piston head[20]. Spherical tanks are used for large buoyancy changes, at high depths of operation and are easier to integrate with AUVs that are normally torpedo-shaped. In our design, a tank has finite volume and it can have: (1) all water, (2) all air, and (3) some water and some air. We use only the condition of (3) and we do not advocate the usages of (1) and (2) because for: (1) Failure can happen because of compression buckling resulting from suction effect when removing the water and (2) lower density of air will not result into in buoyancy change.

Based on the requirement of change in buoyancy (ΔB) in kg and then the inner volume (V_{inner}) of the tank in the cubic meter is computed as:

$$V_{inner} = \Delta B \Big/ \left(\eta_v \rho_f\right) \tag{3}$$

where η_v is the volumetric efficiency (i.e. ratio of the volume of the ballast tank that can be filled to the maximum volume of the ballast tank) and ρ_f is the fluid density (i.e. in our application liquid) in kg/m^3. Further, to decrease the buoyancy of vehicles, ballast tanks are filled, and based on the assumption that the ballast tank completely pressures tight then the volume of air inside the tank remains the same and pressure will increase on the addition of the water inside the ballast tank.

Following Woods[21], *et al.* under the assumption of an ideal gas (e.g. air in this case), an increase in the pressure can be computed by Boyle's law as:

$$\begin{aligned} P_a V_{inner} = P_2 V_2 \Rightarrow P_2 &= \frac{P_a \times V_{inner}}{V_2} \\ &= \frac{P_a \times V_{inner}}{(V_{inner} - V_{ff})} = \frac{P_a}{(1 - V_{ff} / V_{inner})} \end{aligned} \tag{4}$$

where P_a is the atmospheric pressure (i.e. initial pressure inside the ballast tank), P_2 is the air compressed pressure, V_2 is the volume of air occupied after filling of the fluid in the ballast tank, and V_{ff} is the volume of the fluid-filled in the ballast tank. A CAD model of the VBS in the standalone mode is shown in Fig. 5(a). Variation of pressure versus the mass of water added to the ballast tank of (i.e. inner volume $V_{inner} = 0.0071\ m^3$) of buoyancy capacity 7.24 kg is shown in Fig. 5(b). From these results, it can be observed that after filling 5.3 kg of water into the ballast tank the pressure will increase to 3.77 bar pressure. Because as the mass of water inside the tank approaches higher values such as 5 or 6 kg then the pressure inside the tank increases rapidly. It reaches even higher values further because the pressure increases exponentially towards infinity (because of the extremely low value in the denominator) when the maximum inner volume of the ballast tank is filled with water and approaches to 7.24 kg. Since the ballast tank considered here are thin-walled only, we compute the critical pressure[22] as follows:

$$P_{cr} = \frac{2E_m}{\sqrt{3(1-\nu^2)}} \left(\frac{t}{R_m}\right)^2 \tag{5}$$

where E_m is the elastic modulus, ν is the Poisson's ratio (i.e. the property of the material), t is the thickness of the ballast

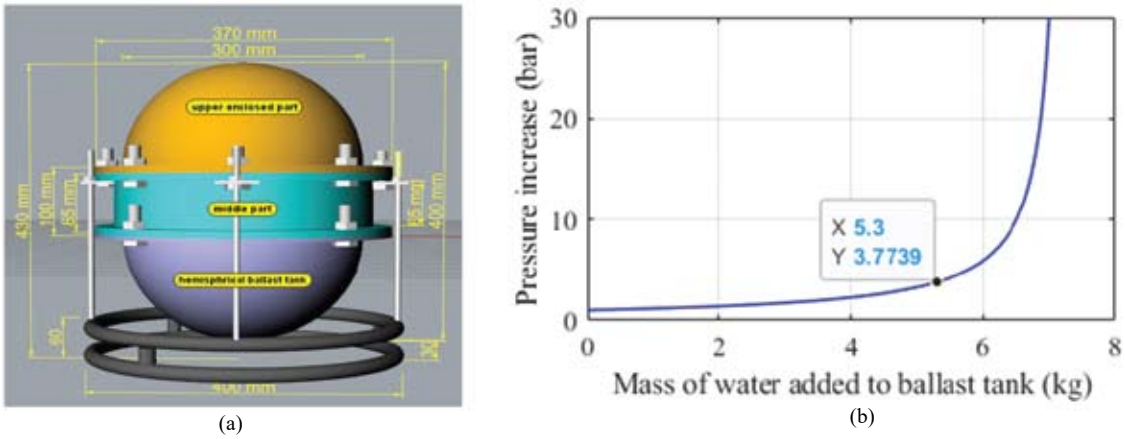

(a) (b)

Figure 5. (a) CAD model of the VBS in standalone mode and (b) Variation of the mass of water added to the ballast tank versus pressure rise in the tank.

tank, and R_m is the mean radius of the ballast tank. Ballast tanks need to be analysed for buckling that is governed by E_m, t, R_m *and* ν. In our application, we prefer high E_m / ρ because the idea is to have a low mass of the VBS to avoid a reduction in the UV's payload. We focus on the design and development of the VBS in standalone mode and it is designed into three modular components, 1) Bottom part as a hemispherical ballast tank (pressure-tight with circular PVC disk of 0.010 m thickness); 2) Middle part to keep the battery, pumps flow sensors and control units, etc. and 3) Upper enclosed part. Because of an increase in the pressure inside the ballast tank by adding the water in it, a significantly high force will act on the tank and disk. To address this, a pressure check/relief valve is used and it is open to the fluid (i.e. in our application liquid) medium. Furthermore, after removing the water from the ballast tank to make it positively buoyant, a high compressive suction force will be created and that is resisted either by adding the same amount of air to the tank from an onboard compressed air cylinder/chamber or by using the high strength material.

The selection of material for the ballast tank is considered based on two criteria: high yield strength to density ratio and high modulus of elasticity along with sufficient thickness. A high modulus of elasticity along with sufficient thickness will tend to prevent buckling. High yield strength to density ratio will result in low system weight and high net effective payload. So we explore different material alternatives and their strength analyses for the ballast tank of VBS are listed in Table 1. From these results, we can observe that the GFRP is the best suitable option for the selection of the material for the ballast tank because of its high compressive yield strength and low density. Nevertheless, we also note here that our analysis has focused primarily on compression because that is dominating under the high hydrostatic pressure and we do not consider the cost aspect. For the given specification of the ballast tank (i.e. t = 0.006 m, and R_m = 0.156 m) it has the critical pressure of 128.0 MPa which is greater than the hydrostatic pressure acting on the ballast tank. Hence, it is not susceptible to buckling.

4. COMPONENT WISE RECORD AND ANALYSIS OF THE MECHANICAL AND ELECTRONIC SYSTEMS OF VBS

4.1 Electronic Components used for Computation of the Amount of Water Filled/Emptied inside the Ballast Tank and Depth Measurements

Herein, we use the method of change in buoyancy by changing the mass of the vehicle, and to compute the exact amount of water that needs to be filled/removed from the ballast tank, the following two methods can be used:

- By using the water level sensor based on assumption that the water level is horizontal only and with this the volume of water added (V_{wa}) inside the ballast tank can be computed as:

$$V_{wa} = \pi\left[-\frac{h^3}{3} + (R_t - h_0)h^2 + \left(2R_t - h_0^{\,2}\right)h\right] - \pi R_{is}^2 (h - h_1) - V_0 \tag{6}$$

$$h_0 = \sqrt{R_t^2 - R_2^2} \tag{7}$$

where h is the water level height inside the ballast tank (we assume that the water level inside the ballast tank remains horizontal while neglecting the effect of sloshing), R_t is the

Table 1. Different material properties for strength analyses of ballast tank of VBS in standalone mode adapted from MPD[23]

Material for the ballast tank	Density (kg/m^3)	Elastic modulus (GPa)	Poisson's ratio (ν)	Compressive yield strength (MPa)	Critical pressure (MPa)
ASTM A36 grade steel	7850	200	0.26	152	353.8
Titanium Alloy (Ti-6AI-4V)	4430	113.8	0.34	970	206.7
Aluminum alloy (7178-T6)	2830	71.7	0.33	530	129.7
GFRP (Epoxy/S-glass uni-directional)	1830	73.1	0.22	1200	128.0

inner radius of the ballast tank, h_1 is the distance between the bottom of the ballast tank and the liquid level sensor, V_0 is the volume of the floating ball inside the ballast tank and R_{is} is the radius of the inner rod connected to the liquid level sensor. Another method is by using the water flow sensor and in this study, we use this. Variation of the buoyancy change rate versus voltage supplied to the pump using the water flow sensor to measure the flow rate during filling/emptying the ballast tank is shown in Fig. 6(a). Herein we have used a water flow sensor to measure the flow rate achieved by the pump at different input voltage supplied to the pump. As the pump flow rate is a function of the voltage supplied, specific supplied voltage results into a specific flow rate.

- Herein, the depth of the VBS in standalone mode is measured using the pressure sensor. It measures the hydrostatic pressure of the water body (i.e. applicable up to 15 bar, 150 m depth of hydrostatic pressure) and this measurement of the pressure leads to the depth rating of the system. The calibration of the 'Water Pressure Sensor (WPS)' is shown in Fig. 6(b) and developed VBS is shown in 6(c). The calibration of the pressure sensor offset voltage (V_{offset}) for its zero pressure is done at the initial stage and the pressure sensor signal is checked in terms of the sensor output voltage. This is noted as the following:

$$V_S = \text{analogRead}(A0) \tag{8}$$

where V_S is the sensor value in the range of 0 – 1023 and the output voltage of the sensor (V_{sensor}) in the range of the 0 to 5 volt can be computed as:

$$V_{sensor} = \left(\frac{5}{1023}\right) V_S \tag{9}$$

Further from the design specifications of the pressure sensor, the pressure is the linear function of the sensor signal (i.e. sensor output voltage) and the slope of it is 0.4 MPa /volt, so the pressure in terms of the voltage can be written as the following:

$$P = (V_{sensor} - V_{offset}) \times 0.4 \tag{10}$$

where P is the pressure in MPa, and it is taken from the specifications of the pressure transducer. With these inputs the operating depth (H_{op}) is computed as the following:

$$H_{op} = P / \rho_f g \tag{11}$$

where ρ_f is the density of the fluid (i.e. in our application liquid) and g is the gravitational acceleration.

4.2 Internal Hardware Connection for Various Components of the Variable Buoyancy System

Integrated and detailed system architecture for various components of VBS is shown in Fig. 7. We use a diaphragm positive displacement water pump of 12 V DC supply with the self-priming property and it can be operated up to 6.8 bars. In our design we have used electric diaphragm type PDP because of the following reasons: Small in size, lower weight, self-priming ability, and high efficiency. Nevertheless, we also note its limitations as the following:

(a) Low operating pressure: Although diaphragm pumps are applicable up to 1000 bar, the one we have considered is applicable up to 60 m depth, and

(b) Maximum flow rate is 4.5 kg/min.

The flow rate of this pump at nominal 12 V is 4.5 'Liter Per Minute (LPM)' and the range of the voltage varies from 9 to 14 V to control the flow rate of water in this range of voltage. Generic A3-7IRU-ZZN0 electric solenoid valve (i.e. operating at 12 V DC) is used for energising or de-energising to allow the flow of the fluid or stop the flow in the desired direction.

4.3 Stability Analysis of VBS in Standalone Mode

To investigate the static stability of the submerged body, we consider the Center of Gravity (CG) and the Center of Buoyancy (CB). We design the system to ensure that the CG is below the CB. The CB is also the geometric center for the symmetrical submerged body's section. In our work, the designed and developed VBS in standalone mode is symmetrical in its geometric shape under submerged conditions. Therefore the CB will be at the geometric center of the system (i.e. while neglecting the effect of circular ring on the CB). To test the VBS in the standalone mode, we have attached two circular iron rings with four vertical rods that are connected to the system. These arrangements of rings and rods are needed to ensure that the VBS has sufficient contact area and to alter the

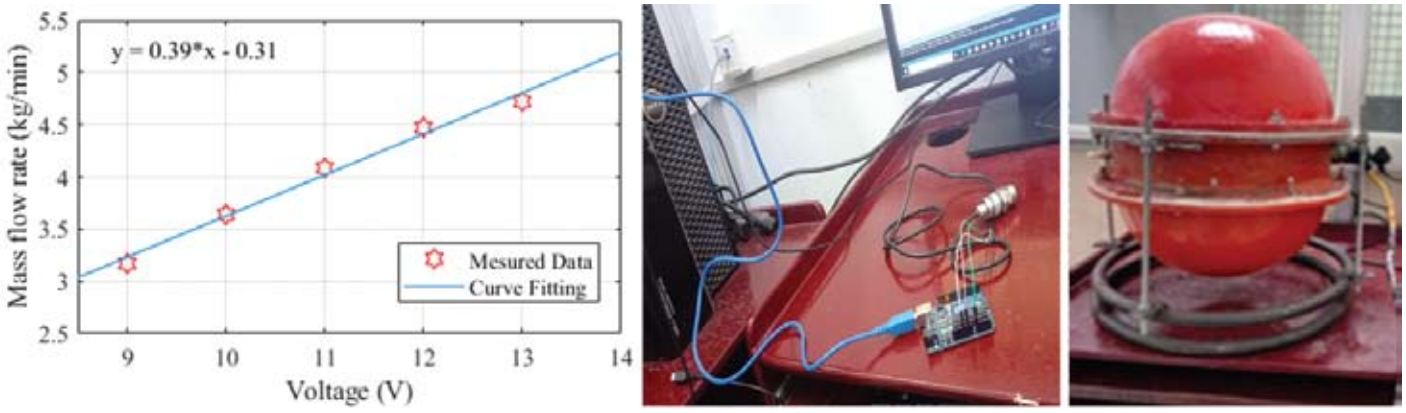

(a) (b) (c)

Figure 6. (a) Buoyancy change rate versus voltage supplied to the pump, (b) Calibration of the pressure sensor, and (c) Developed VBS.

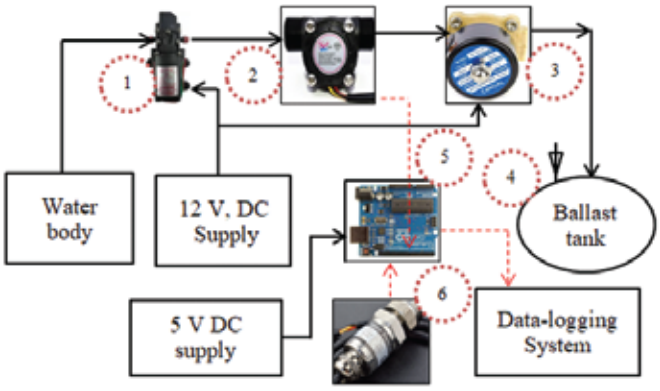

Figure 7. Integrated and detailed system architecture for various components of the VBS where 1 - Positive displacement diaphragm pumps, 2 - flow measured sensor, 3 - solenoid valve, 4 - pressure relief valve, 5 - microcontroller, and 6 - water pressure sensor.

mass distribution of the VBS to bring the CG closer to the base. We note that these arrangements are only applicable in the VBS in standalone mode, and when the VBS is integrated with UV these will not be needed. We compute the CG for VBS in the vertical direction as follows:

$$z_{CG} = \sum_{i=1}^{n} m_i z_i \Big/ \sum_{i=1}^{n} m_i \tag{12}$$

where m_i is the mass of ith component, z_i is the vertical distance of ith component, and n is the total number of components. The computed value of z_{CG} is 5 cm below the geometric center and with this, we note that the VBS is statically stable. Nevertheless, the dynamic stability of the developed VBS integrated with the UV has not been focused upon in the current work.

5. PERFORMANCE ANALYSIS OF THE VBS IN STAND-ALONE MODE

To analyse the performance of the VBS in standalone mode through computer simulation, the mathematical model of VBS can be written as follows:

$$ma = F_G - F_B - F_D - F_a = \left(m - \rho_f V_{di}\right)g - \frac{1}{2} C_D \rho_f A_p |w| w - m_a a \tag{13}$$

where m is the mass of VBS, F_G is the gravitational force, F_B is the buoyancy force, F_D is the drag force, g is the gravitational acceleration, ρ_f is the density of the liquid in which the VBS is operating, V_{di} is the displaced volume by VBS, C_D is the drag coefficient, w is the velocity in the vertical plane (i.e. heave velocity), m_a is the added mass and a is the acceleration of VBS. Assuming, that the change in buoyancy is as follows:

$$\Delta B = \left(m - \rho_f V_{di}\right) \tag{14}$$

Implying that it is neutrally buoyant when $\Delta B = 0$, positively buoyant if $\Delta B < 0$, and negatively buoyant if $\Delta B > 0$). Now, we get the following:

$$\left(m + m_a\right)a = \Delta B g - \frac{1}{2} C_D \rho_f A_p |w| w \tag{15}$$

$$a = \frac{\left(-1/2\, C_D \rho_f A_p |w| w\right)}{\left(m + m_a\right)} + \frac{\Delta B g}{\left(m + m_a\right)} \tag{16}$$

$$\dot{w} = -\frac{C_D \rho_f A_p |w| w}{2\left(m + m_a\right)} + \frac{\Delta B g}{\left(m + m_a\right)} \tag{17}$$

$$\dot{z} = w \tag{18}$$

where $\dot{z}$ is the rate of change of depth and all other parameters are the same as defined before. Following Fossen[24] the added mass is computed based on the assumption that the shape of VBS is a prolate ellipsoid. Other simulation parameters of the VBS in the standalone mode are listed in Table 2. Furthermore, we limit our application range to less than 100 m, and across this water depth, the water density does not change significantly; for more details see Gladkikh[25]. Therefore we have not considered the effect of depth on density in the present work.

Table 2. Simulation parameters of the VBS in the standalone mode

Parameter	Value	Unit
m	26.65	kg
m_a	11.2	kg
A_p	0.098	m^2
C_D	0.8	-
g	9.81	m/s^2
ρ_f	1025	kg/m^3
V_{di}	0.026	m^3

Open-loop simulation results of heave velocity versus time for three different buoyancy capacities i.e. 1.0, 1.5, and 2.0 kg, and the VBS in the standalone mode achieves the terminal velocity of 0.49, 0.6, and 0.71 m/s respectively are in Fig. 8(a). Figure 8(b) shows the depth versus time of VBS in standalone mode and from these results, we observe that the system reaches 60 m depth in 85 sec for 2 kg buoyancy change and takes 122 s for reaching the same depth with 1 kg buoyancy change.

5.1 Validation of the present simulation-based results

For the validation, we compare our results with the existing design performance results of the Underwater Robotic Vehicle (URV), Sumantr[16], *et al.* Figure 8 shows the comparison of simulation-based performance analysis of our developed VBS in standalone mode with simulation results of URV of Sumantr[16], *et al.* Our results follow the same trend and they match qualitatively. The maximum heave speed achieved by us is lower than Sumantr URV and this is mainly because of higher drag. Our results differ from Sumantr URV at the quantitative level because of multiple reasons, e.g. URV's spherical shape, size, they have not reported the coefficient of drag; their buoyancy change is 1.019 kg (10 N); and their mass is lower than the mass of our VBS, etc.

Furthermore, we have analysed the amount of reduction in energy consumption due to the use of VBS and we consider

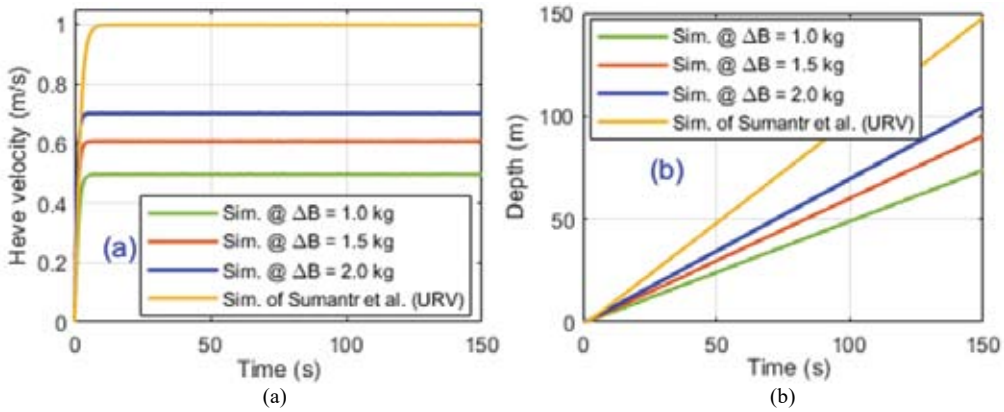

Figure 8. Comparison of simulation-based performance analysis of our developed VBS in standalone mode with URV of Sumantr[16], *et al.* (a) Open-loop simulation results of heave velocity versus time; - (b) Variation of depth versus time of VBS.

two cases: Case 1 - Vehicle operated with buoyancy control and Case 2 - VBS as the vehicle operated with the thruster. Results are as follows:

- Case 1: Energy consumption by the VBS during the change in buoyancy at any given depth of operation is a function of net buoyancy change required and operating depth. This can be written as follows:

$$E = \Delta B \times g \times H_{op} \tag{19}$$

where ΔB is the needed net buoyancy change at an operating depth (H_{op}) and g is the gravitational acceleration. We consider three buoyancy changes, e.g. ΔB = 1, 1.5 and 2.0 kg. For these, the variation of energy required versus operating depth with developed VBS in standalone mode is shown Fig. 9 (a).

- Case 2: In this, we analyse the energy (E) required by the propeller to overcome the drag acting on the vehicle when it is operating across the depth range of H_{op} m and moving with heave velocity w. Required E can be written as follows:

$$E = \left(\frac{0.5 \rho_f w^2 C_D A_p H_{op}}{\eta_{prop}} \right) + E_0 \tag{20}$$

where E_0 is the no-load condition (i.e. for rotating the propeller alone in the free condition means during the lab testing of the free running of the propeller) and other energy loss components, η_{prop} is the propeller efficiency, C_D is the drag coefficient, ρ_f is the density of the fluid (i.e. in our application liquid) in which the propeller is operating and A_p is the projected area of the vehicle. Herein, to analyse the performance of the vehicle, we consider the following simulation parameters: E_0 = 40 J and η_{prop} = 0.8. All other parameters are the same as defined previously in Table 2.

Herein, to quantify the reduction of energy using VBS in comparison with the thruster we consider operating the vehicle at the same heave velocity, i.e. achieved by a change in buoyancy and achieved by using the thruster. Figure 9(b) shows the variation of the energy required versus operating depth with a propeller for designed VBS in standalone mode. From these results, we observe that for 60 m depth of operation, energy consumption by the VBS in standalone mode is around 20 % less when operating with 2 kg of negative buoyancy than the propeller to descend at the same speed of 0.71 m/s for each cycle. Furthermore, as the depth is increasing the energy required by the propeller increases more than the required increase of energy for change in buoyancy by using the VBS. Because of this even, more than 20 % reduction of energy consumption is noted for the larger depths of operation. Reduction in the energy consumption for depth control, and

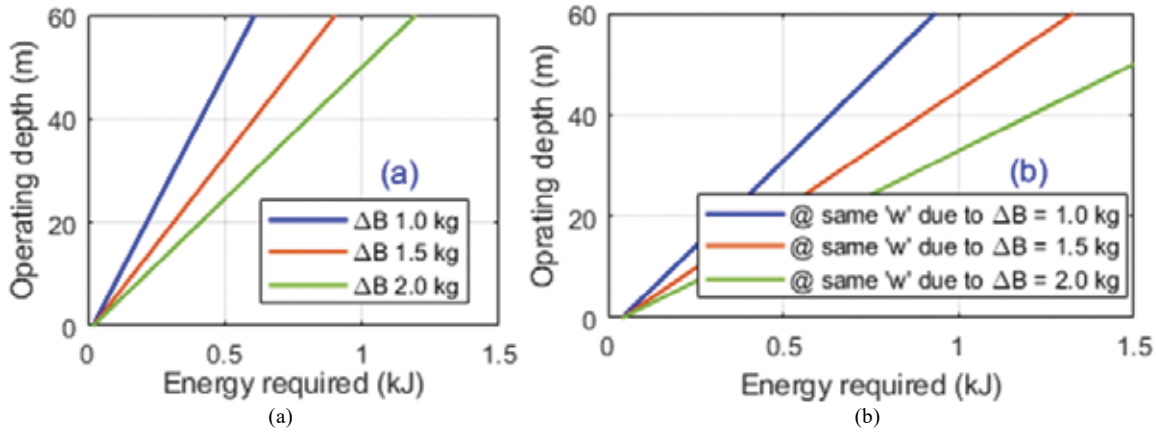

Figure 9. (a) Variation of energy required versus operating depth with VBS and (b) Variation of energy required versus operating depth with the propeller for the designed VBS in standalone mode at different heave velocities (w).

change in the buoyancy in the order of 20 % and higher, justify the design, development, and application of VBS in UVs as compared to the use of propeller for the same usages.

6. CONCLUSIONS

This paper presented the design and analysis of the VBS for depth control of UVs and discussed the details of the system architecture of various components of the VBS required for fabrication and experimental verification. The buoyancy capacity of the developed VBS is $\pm\Delta B = 5$ kg and herein numerical simulation of the VBS in standalone mode was reported in the open-loop. Work presented in this paper is applicable up to 60 m depth and has been designed to be directly installed in medium-size UVs. Simulation results show that the developed VBS can reduce up to 20 % of energy consumption for each cycle (i.e. descending and ascending), in comparison to the same VBS being operated in standalone mode with either propeller or thruster for 60 m depth of operation. However, we have not reported experimental verification studies and their comparison with simulation results is yet to be investigated.

Buoyancy changes if we move from river to lake to sea to ocean because each will have its own water density and other properties. Similarly, in the descent move if the UV goes to deep then the effect of depth on seawater density will come into the computation. At present, our application range has been less than 100 m and across this water depth, the water density does not change significantly. Nevertheless, for higher depth applications this needs to be considered. These are currently being investigated by us and are expected to be reported shortly in near future.

REFERENCES

1. Tiwari, B.K. & Sharma, R. A computing model for design of flexible buoyancy system for autonomous underwater vehicles and gliders. *Def. Sci. J.*, 2019, **68**(6), 589-596. doi: 10.14429/dsj.68.12548
2. Davis, R. E.; Eriksen, C. C. & Jones, C. P. Autonomous buoyancy-driven underwater gliders. *In* Technology and Applications of Autonomous Underwater Vehicles, edited by G. Griffiths, Taylor and Francis, New York, London, UK, 2003, pp. 37-58. doi: 10.1201/9780203522301.ch3
3. Griffiths, G.; Jamieson, J.; Mitchell, S. & Rutherford, K. Energy storage for long endurance AUVs. *In* Proceedings of Advances in Technology for Underwater Vehicles, London, UK, 2004, pp. 8–16.
4. Bradley, A. M.; Feezor, M. D.; Singh H. & Sorrell F. Y. Power systems for autonomous underwater vehicles. *IEEE J. Oceanic Eng.*, 2001, **26**(4), 526-538. doi: 10.1109/48.972089
5. Dzielski, J.E.; Tangirala, C.; Moyer, W.W. & Bradley, D.L. NAVOCEANO Seahorse AUV design, testing, and capabilities. *In* Proceedings of MTS/IEEE Oceans Conference & Exhibition, Biloxi, USA, 2002, pp. 151–155. doi: 10.1109/OCEANS.2002.1193263
6. Hyakudome, T.; Aoki, T.; Murashima, T.; Tsukioka, S.; Yoshida, H.; Nakajoh, H.; Ida T.; Ishibashi, S. & Sasamoto, R. Key technologies for AUV URASHIMA. *In*, Proceedings of MTS/IEEE Oceans Conference, Biloxi, USA, 2002, pp. 162–166. doi: 10.1109/OCEANS.2002.1193265
7. Thorleifson, J. M.; Davies, T. C.; Black, M. R.; Hopkin, D. A.; Verrall, R. I.; Pope, A.; Monteith, I.; Den H. V. & Butler, B. The Theseus autonomous underwater vehicle. A Canadian success story. *In* Proceedings of the MTS/IEEE Oceans Conference, Halifax, Canada, 1997, pp. 1001-1006. doi: 10.1109/OCEANS.1997.624127
8. Wu, J.; Liu, J. & Xu, H. A variable buoyancy system and a recovery system developed for a deep-sea AUV Qianlong I. *In* Proceedings of IEEE Oceans Conference, Taipei, 2014, pp. 1-4. doi: 10.1109/OCEANS-TAIPEI.2014.6964315
9. Song, D.; Qin, S.; Sun, W.; Jiang, Q. & Yang, H. Research of an accurate buoyancy adjusting method of underwater glider based on temperature compensation. *In* Proceedings of IEEE Oceans Conference, Aberdeen, UK, 2017, pp. 1-5. doi: 10.1109/OCEANSE.2017.8084638
10. Huang, Y.; Wang, Z.; Yu, J.; Zhang, A.; Qiao, J. & Feng, H. Development and experiments of the passive buoyancy balance system for sea-whale 2000 AUV. *In* Proceedings of IEEE Oceans Conference, Marseille, France, 2019, pp. 1-5. doi: 10.1109/OCEANSE.2019.8867151
11. Wang, Z.; Yu, J.; Zhang, A.; Sun, Z. & Kang, S. Development and experiments of the buoyancy adjusting system of long-range AUV. *In* Proceedings of MTS/IEEE Oceans, Kobe Techno-Oceans (KTO), Kobe, 2018, pp. 1-6. doi: 10.1109/OCEANSKOBE.2018.8559046
12. Eriksen, C.C.; Osse, T.J.; Light, T.; Wen, R.D.; Lehmann, T.W.; Sabin, P.L. & Ballard J.W. Seaglider: a long range autonomous underwater vehicle for oceanographic research. *IEEE J. Oceanic Eng.*, 2001, **26**(4), 424–436. doi: 10.1109/48.972073
13. Douglas, C.W.; Simonetti, P.J. & Jones, C.P. SLOCUM: An underwater glider propelled by environmental energy. *IEEE J. Oceanic Eng.*, 2001, **26**(4), 447–453. doi: 10.1109/48.972077
14. Shibuya, K.; Kishimoto, Y. & Yoshii, S. Depth control of underwater robot with metal bellows mechanism for buoyancy control device utilizing phase transition. *J. Robotics Mechatronics*, 2013, **25** (5), 795-803. doi: 10.20965/jrm.2013.p0795
15. Ranganathan, T.; Singh, V.; Nair, R. & Thondiyath, A. Design of a controllable variable buoyancy module and its performance analysis as a cascaded system for selective underwater deployment. *Proc. IMechE Part M: J. Eng. Maritime Environ.*, 2017, **231** (4), 888-901. doi: 10.1007/s00773-018-0599-2
16. Sumantr, B.; Karsiti, M.N. & Agustiawan, H. Development of variable ballast mechanism for depth positioning of spherical URV. *In* the proceedings of the IEEE International Symposium on Information Technology, Kuala Lumpur,

Malaysia, 2008, pp. 1-6.
doi: 10.1109/ITSIM.2008.4631898

17. Zhang, H.; Zhang, J.; Liu, Y.; Wang, Y.; Wang, S.; Wu, Z. & Zheng, Y. Research on the influence of balance weight parameters on the motion performance of the seafloor mapping AUV in vertical plane. *Ocean Engineering*, 2015, **109**, 217-225.
doi: 10.1016/j.oceaneng.2015.09.015
18. Ayyangar, V.B.S.; Krishnankutty, P.; Korulla, M. & Panigrahi P.K. Stability analysis of a positively buoyant underwater vehicle in vertical plane for a level flight at varying buoyancy, BG and speeds. *Ocean Engineering*, 2018, **148**, 331-348.
doi: 10.1016/j.oceaneng.2017.11.030
19. Wang, S.; Li, H.; Wang, Y.; Liu, Y.; Zhang, H. & Yang, S. Dynamic modeling and motion analysis for a dual-buoyancy-driven full ocean depth glider. *Ocean Engineering*, 2019, **187**, 1-11.
doi: 10.1016/j.oceaneng.2019.106163
20. Wang, W. H.; Engelaar, R. C.; Chen, X. Q. & Chase J. G. The state-of-art of underwater vehicles-theories and applications. *In* Proceedings of Mobile Robots-State of the Art in Land, Sea, Air, and Collaborative Missions, edited by X.Q. Chen, Y.Q. Chen and J.G. Chase, IntechOpen, 2009, pp. 129-152.
doi: 10.5772/6992
21. Woods, S. A.; Bauer, R. J. & Seto, M. L. Automated ballast tank control system for autonomous underwater vehicles. *IEEE J. Oceanic Eng.,* 2012, **37**(4), 727-739.
doi: 10.1109/JOE.2012.2205313
22. Pan B. & Cui W. An overview of buckling and ultimate strength of spherical pressure hull under external pressure. *Marine Struct.*, 2010, **23**(3), 227-240.
doi: 10.1016/j.marstruc.2010.07.005
23. MPD, ASM Material Data Sheet References, Met Web, USA, website address: www.matweb.com, (Accessed on July 9, 2020).
24. Fossen, T.I. Guidance and control of ocean vehicle, John Wiley & Sons, USA, 1999.
25. Gladkikh, V. & Tenzer, R. A mathematical model of the global ocean saltwater density distribution. *Pure Appl. Geophys.*, 2012, **16** (12), 249-257.
doi: 10.1007/s00024-011-0275-5

ACKNOWLEDGEMENT

This research was supported by the internal research grants of IIT Madras through research scheme: OE14D212 and from Marine Systems Panel, NRB, India via a sponsored project: NRB-263/MAR/12-13.

CONTRIBUTORS

Mr B.K. Tiwari received his BSc (Physics, Chemistry and Mathematics) from the Avadh University, Ayodhya, India, in 2007 and BE (Aeronautical engineering) from the Aeronautical Society of India, in 2013. Currently, he is in the final stage of his PhD at the Department of Ocean Engineering, Indian Institute of Technology Madras, Chennai, India. His research interests are: Design and development of autonomous underwater vehicles and gliders, guidance and control of marine vehicles, marine robotics and mathematical modelling and simulation.
In the current study, he has implemented the formulation, performed all the analyses and prepared the final manuscript.

Dr R. Sharma received his BE (Civil Engineering) from the Indian Institute of Technology, Roorkee (formerly University of Roorkee) in 1994; MTech (Ocean Engineering) in 1999 and PhD from the Indian Institute of Technology Kharagpur, India, in 2008. Presently, he is working as Professor in the Department of Ocean Engineering, Indian Institute of Technology madras, Chennai, India. His research interests are: Design, analysis and production of marine structures, marine robotics and dynamic data driven forecasting systems.
In the current study, he has conceived the problem, provided overall guidance and supervision in the current study.